Available online at www.sciencedirect.com
ScienceDirect
Journal of Sound and Vibration 309 (2008) 739–755
JOURNAL OF SOUND AND VIBRATION
www.elsevier.com/locate/jsvi

On the railway track dynamics with rail vibration absorber for noise reduction

T.X. Wu*

State Key Laboratory of Mechanical System and Vibration, Shanghai Jiao Tong University, Shanghai 200240, PR China

Received 13 April 2007; received in revised form 29 June 2007; accepted 28 July 2007
Available online 19 September 2007

Abstract

A promising means to increase the decay rate of vibration along the rail is using a rail absorber for noise reduction. Compound track models with the tuned rail absorber are developed for investigation of the performance of the absorber on vibration reduction. Through analysis of the track dynamics with the rail absorber some guidelines are given on selection of the types and parameters for the rail absorber. It is found that a large active mass used in the absorber is beneficial to increase the decay rate of rail vibration. The effectiveness of the piecewise continuous absorber is moderate compared with the discrete absorber installed in the middle of sleeper span or at a sleeper. The most effective installation position for the discrete absorber is in the middle of sleeper span. Over high or over low loss factor of the damping material used in the absorber may degrade the performance on vibration reduction.

1. Introduction

Railway is seen as a means of environmental-friendly transportation by providing clean and efficient mass transit. However, noise and vibration problems due to railway operation become public, technical and administrative concern. The predominant source of noise from railway is associated with the rolling of the wheel on the rail. The roughness on the wheel and rail tread forms excitation and causes vibration of the wheel and track. When vibration propagates in the wheel and rail, the structure radiates noise.

Theoretical models have been developed for understanding and predicting rolling noise, and these have been validated in extensive field measurements [1–5]. The sound radiated by the wheel is the most important component at high frequencies, above about 1.5 kHz, the sound from the rail dominates in the middle frequency range 500–1500 Hz and at low frequencies, sound radiated by the sleepers dominates. Rail radiation is one of the significant sources of rolling noise. The main parameter with the strongest influence on the amount of noise radiated by the rail is the rate of decay of vibration in the vertical direction along the rail, usually expressed in dB/m [6]. A doubling of decay rate in a particular frequency band leads to a reduction of noise from the rail by 3 dB in that band [7]. The rail pad stiffness is of particular importance for the decay rate and track component of noise [8]. Theoretical studies have shown that stiff pads increase the decay rate and

*Tel.: +86 21 3420 6332x819; fax: +86 21 3420 6006.
E-mail address: txwu@sjtu.edu.cn

0022-460X/$ - see front matter © 2007 Elsevier Ltd. All rights reserved.
doi:10.1016/j.jsv.2007.07.049

thus decrease the rail noise, whereas soft pads lead to low decay rate and increase the rail noise [9]. In recent years, however, soft pads have become commonly applied to reduce track forces and consequently damage to the track components.

Alternative ways adding damping to the rail have been developed. A promising means to increase the decay rate of vibration along the rail is using a rail damper. A reduction of 6 dB in track component of rolling noise was achieved in the tests by using a two-layer tuned absorber system attached continuously to the rail on each side [10]. The main benefit of such a rail absorber/damper is to allow soft rail pads to be used for reducing dynamic loads to the track components, without any increase in noise levels. A similar rail damper but concentrated in shorter, wider units was tested [11], which are clipped onto the rail between sleepers. A reduction of 3 dB in overall noise was found in tests on a running line with pads of medium stiffness about 350 MN/m. A so-called "double tuned rail damper" was developed to suppress the pinned–pinned resonance, which is mounted between two sleepers on the rail [12]. Measurements showed that the decay rate of rail vibration can effectively be improved by the rail damper in the frequency range 500–2500 Hz.

Although measurement results and models of the rail with the absorber/damper can be referred to and some types of rail damper products are patented or commercially available [10–12], comprehensive study on the track dynamics with the rail absorber seems not to be sufficient. The purpose of this study is to obtain better understanding of the mechanism of the rail absorber through detailed investigation into the dynamic properties of the track combined with the absorber and, to gain some guidelines on selection of the types and parameters of the rail absorber to achieve better performance on noise reduction.

Firstly, the mechanism of energy consumption by the rail absorber is briefly introduced. Then a continuous model of the track combined with the rail absorber is developed, which is modelled as a two-degrees-of-freedom vibration system continuously attached to the rail, for analysis of vertical dynamics of the track. Using the combined track model the influences on decay of rail vibration are investigated of the parameters of the absorber. Afterwards a discrete track model is developed combined with either the continuous or the discrete rail absorber to calculate their difference in the effectiveness on decay of track vibration. Finally, the influence on vibration decay is studied of the installation positions for the discrete absorber, which are chosen to be in the middle of sleeper span and at a sleeper. The simulation results show that a large active mass used in the absorber is beneficial to decay of rail vibration. Over high or over low loss factor of the damping material used in the absorber are not appropriate for vibration reduction. The most effective installation position for the discrete absorber is in the middle of sleeper span, because where the amplitude of rail vibration is high and the pinned–pinned resonance can effectively be damped. As the vibration amplitude is flat at a sleeper, it is not an appropriate place for arranging the discrete absorber. The effectiveness of the piecewise continuous absorber installed along the rail is moderate, compared with the discrete absorber installed in the middle of sleeper span or at a sleeper.

2. Basic analysis of track dynamics with rail absorber

In this section, the mechanism of the rail absorber reducing vibration and radiation is introduced using a continuous track model. In addition, the effects on decay of rail vibration are investigated of the parameters of the rail absorber, in order to establish a baseline for their selection to achieve good performance on rail noise reduction at the source when designing the absorber.

2.1. Mechanism of rail absorber

The rail absorber studied consists of the steel mass bars and the elastomeric material layers between them and the rail. The elastomeric layers are glued to the lower part of the rail web and the upper surface of the rail foot, as shown in Fig. 1. The absorber is attached to each side of the rail web, and may be either piecewise continuous or discrete along the rail. However, it is not always the case and other products exist, using masses and elastomeric layers, which look different.

The rail absorber works as a vibration system of two degrees of freedom when the mass-bar is short, for example less than 0.15 m in length. Under this condition, the mass-bar can approximately be regarded as a rigid body because its natural frequencies of bending vibration are above 3 kHz for the parameters used in the

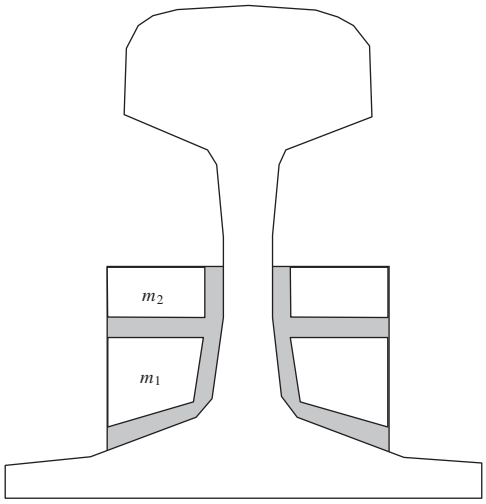

Fig. 1. Cross-section of the rail with absorber [10].

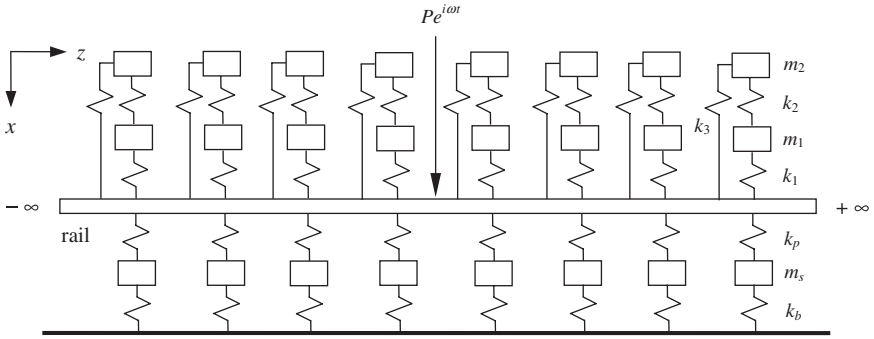

Fig. 2. Railway track model with rail absorber.

study. Fig. 2 shows the railway track model with the rail absorber, which is for the vertical vibration and to be presented in details later. The upper parts above the rail represent the absorber, and the lower parts under the rail are the rail support composed by the rail pad, sleeper and ballast. In the upper parts, the absorber is modeled to be composed of the compound mass–spring layers without considering the bending stiffness of the mass bar, where m_1 and m_2 represents the bottom and upper mass of the absorber, respectively, k_1 represents the stiffness of the elastomeric layers between the bottom mass and the rail, k_2 represents the stiffness of the elastomeric connection between the upper and bottom mass and k_3 is the elastomeric connection between the upper mass and the rail. k_3 may be equal to zero if the connection between the upper mass and the rail is structurally disconnected. k_1, k_2 and k_3 are all complex with loss factor η_a. At the first-order vibration mode the upper and bottom masses of the absorber oscillate up and down in phase, whereas at the second mode they oscillate out of phase.

The parameters of the absorber should be selected such that the vibration magnitude is small of the upper mass, but large of the bottom mass at the second resonance. Fig. 3 shows the vibration transfer ratio from the rail to the absorber mass m_1 and m_2. The first and second resonance frequency of the absorber is designed to be about 250 and 700 Hz, respectively. At the second resonance, it can be seen that the bottom mass of the absorber, m_1, oscillates with large amplitude, whereas the vibration amplitude of the upper mass, m_2, is small compared with the bottom mass, and even smaller than the rail vibration above 400 Hz. In this way, the rail vibration energy can effectively be consumed by the elatomeric material around the second resonance of the absorber, and in the meantime, the upper mass radiates less sound. Therefore, the second resonance frequency

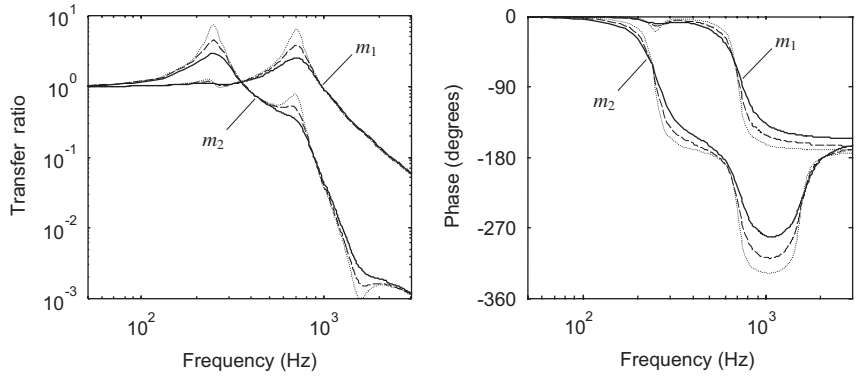

Fig. 3. Vibration transfer ratio of rail absorber with $f_1 = 247$ Hz, $f_2 = 703$ Hz: $\cdots\eta_a = 0.15$, $--\ \eta_a = 0.25$, — $\eta_a = 0.4$.

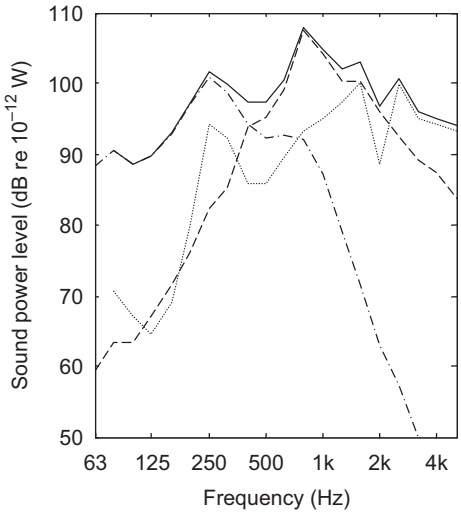

Fig. 4. Example sound power spectra of rolling noise (from Ref. [8]): — total noise, – – rail component, ⋯ wheel component, – · – sleeper component.

of the absorber should be designed to be close to the frequency at which the rail vibration and radiation reach their peaks, so that much energy of rail vibration can be dissipated by the absorber.

Predictions of rolling noise from the TWINS models are shown in Fig. 4 [8]. It can be seen that the main component of rolling noise is from rail radiation, with its peak being at about 650–850 Hz for a train speed 100 km/h and a roughness spectrum corresponding to tread-braked wheels. In practice, the frequency of rail vibration peak varies with the running speed of train, and can be measured in situ.

The resonance frequency of the rail absorber proposed is different from that in Ref. [12], where the lower resonance frequency is approximately equal to the higher resonance frequency of the absorber here. Thus, the active mass of the absorber here is expected to radiate less noise, but at a cost of relatively lower decay rate of rail vibration at high frequencies.

2.2. Continuous track with continuous rail absorber

It is known from the above analysis that the second natural frequency of the rail absorber should be designed to be close to the frequency at which the rail vibration energy level is high. However, many combinations are possible of different mass and stiffness for the absorber to meet the natural frequency requirement. It is therefore important to know the effects on rail vibration attenuation of the mass and

stiffness parameters used for the absorber. To investigate this, a track model with the rail absorber is required to simulate the track dynamics combined with the absorber.

Such a track model for vertical vibration is schematically shown in Fig. 2. The rail is modelled as an infinite Timoshenko beam on the spring–mass–spring layer foundation, and the continuous absorber is modeled as the combined spring–mass layers along the rail. Although there are two single absorbers on both sides of the rail web and they may have different natural frequencies to broaden the frequency range over which the absorber is effective, for simplicity the two absorbers are devised to have the same parameters and natural frequencies and thus can be combined as one absorber. The equations of motion in the frequency domain are given for the rail:

$$-\rho A\omega^2 u + GA\kappa(\phi' - u'') + k_p(u - u_s) + k_1(u - u_1) + k_3(u - u_2) = F\delta(z), \tag{1}$$

$$-\rho I\omega^2 \phi + GA\kappa(\phi - u') - EI\phi'' = 0 \tag{2}$$

for the sleeper

$$-m_s\omega^2 u_s - k_p u + (k_p + k_b)u_s = 0 \tag{3}$$

and for the absorber

$$\begin{bmatrix} k_1 + k_2 - m_1\omega^2 & -k_2 \\ -k_2 & k_2 + k_3 - m_2\omega^2 \end{bmatrix} \begin{Bmatrix} u_1 \\ u_2 \end{Bmatrix} = \begin{Bmatrix} k_1 \\ k_3 \end{Bmatrix} u, \tag{4}$$

where u is the vertical displacement of the beam and ϕ the rotation of the cross-section of the beam due to bending. $\phi - u'$ represents the shear deformation and $'$ indicates the derivative with respect to z, the longitudinal position of the beam. u_s is the displacement of the sleeper mass layer, u_1 and u_2 are the displacement of the bottom and upper mass of the absorber, respectively. F is the amplitude of the harmonic load to the rail, and ω is the circular frequency. The material's properties of the rail are represented by E, the Young's modulus, G, the shear modulus, ρ, the density, and η_r, the loss factor. The geometric properties of the rail cross-section are characterized by A, the cross-sectional area, I, the area moment of inertia and κ, the shear coefficient. For the track support m_s is the sleeper mass density per unit length, k_p and k_b are the pad and ballast stiffness per unit length, respectively. m_1, m_2, k_1, k_2, and k_3 are the parameters of the absorber components and they are described previously. Damping is considered for the rail support and absorber by means of loss factor in the form $k(1 + i\eta)$.

The displacements of the sleeper and absorber masses, u_s, u_1 and u_2, can be solved using Eqs. (3) and (4) in terms of the rail displacement u:

$$u_s = \frac{k_p}{k_p + k_b - m_s\omega^2}\, u, \tag{5}$$

$$u_1 = \frac{k_1(k_2 + k_3 - m_2\omega^2) + k_2k_3}{(k_1 + k_2 - m_1\omega^2)(k_2 + k_3 - m_2\omega^2) - k_2^2}\, u, \tag{6}$$

$$u_2 = \frac{k_3(k_1 + k_2 - m_1\omega^2) + k_1k_2}{(k_1 + k_2 - m_1\omega^2)(k_2 + k_3 - m_2\omega^2) - k_2^2}\, u. \tag{7}$$

Substituting Eqs. (5), (6) and (7) for u_s, u_1 and u_2 in Eq. (1), respectively, results in

$$-\rho A\omega^2 u + GA\kappa(\phi' - u'') + (k_s + k_a)u = F\delta(z), \tag{8}$$

where

$$k_s = k_p\left(1 - \frac{k_p}{k_p + k_b - m_s\omega^2}\right) \tag{9}$$

and

$$k_a = k_1\left\{1 - \frac{k_1(k_2+k_3-m_2\omega^2)+k_2k_3}{(k_1+k_2-m_1\omega^2)(k_2+k_3-m_2\omega^2)-k_2^2}\right\} + k_3\left\{1 - \frac{k_3(k_1+k_2-m_1\omega^2)+k_1k_2}{(k_1+k_2-m_1\omega^2)(k_2+k_3-m_2\omega^2)-k_2^2}\right\} \quad (10)$$

are the dynamic stiffness of the rail support and absorber, respectively.

Eqs. (8) and (2) can be solved by performing the Laplace transform and then the inverse Laplace transform to obtain the rail displacement u. Introducing u into Eqs. (5)–(7) the displacements of the sleeper and absorber masses can be obtained.

Calculations of the track dynamics with the rail absorber are carried out for UIC 60 rail with the continuous track support and absorber. The parameters for the rail are

$$E = 2.1\times10^{11}\,\mathrm{N/m^2},\ \ G = 0.77\times10^{11}\,\mathrm{N/m^2},\ \ \rho = 7850\,\mathrm{kg/m^3},$$
$$\eta_r = 0.01,\ \ A = 7.69\times10^{-3}\,\mathrm{m^2},\ \ I = 30.55\times10^{-6}\,m^4,\ \ \kappa = 0.4.$$

The parameters for the continuous support are

$$k_p = 583\,\mathrm{MN/m^2},\ \ \eta_p = 0.2,\ \ k_b = 83.3\,\mathrm{MN/m^2},\ \ \eta_b = 1.0,\ \ m_s = 270\,\mathrm{kg/m}$$

and the parameters for the absorber are

$$m_1 = 14\,\mathrm{kg/m},\ \ m_2 = 6\,\mathrm{kg/m},\ \ k_1 = 260\,\mathrm{MN/m^2}, k_2 = 12\,\mathrm{MN/m^2},\ \ k_3 = k_2/4,\ \ \eta_a = 0.25,$$

where the stiffness of the elastic connection between the upper mass and the rail, k_3, is chosen to be $k_3 = k_2/4$ for simplicity.

Using the above parameters for the rail absorber its first and second resonance frequencies are calculated to be at about 250 and 700 Hz, respectively.

2.3. Parametric study of track dynamics with absorber

The calculated dynamic properties of the track with the continuous absorber are shown in Fig. 5 in terms of the point receptance (the displacement at the forcing point divided by the force applied), the decay rate of rail vibration along the track and the vibration energy of the rail and the upper mass of the absorber. The vibration energy due to a unit oscillating load applied to the rail at $z = 0$ is evaluated by sum $|v|^2\mathrm{d}z$, where v is the magnitude of vibration velocity and $\mathrm{d}z$ is the length of a small track section.

Comparisons are made in Fig. 5 to the track without the rail absorber. The point receptance of the rail can be seen from Fig. 5 to reach resonance at about 80 and 500 Hz. At 80 Hz, the whole track bounces on the ballast stiffness although this resonance is over-damped, while at 500 Hz the rail vibrates on the pad stiffness. The pinned–pinned resonance does not appear as the rail is continuously supported. A third resonance in the point receptance can be observed at about 900 Hz for the track with the rail absorber. The decay rate of rail vibration is estimated over a 10 m span from the excitation point. It can be seen from Fig. 5 to be moderate at low frequencies and reach a peak 22 dB/m at about 300 Hz. At high frequencies above 700 Hz, if no rail absorber is used, the decay rate is lower than 2 dB/m and even less than 1 dB/m above 1 kHz. When the rail absorber is used, the decay rate of rail vibration is significantly increased in the frequency range 600–1200 Hz, and thus the rail vibration energy can effectively be reduced in that frequency region. This is helpful to rolling noise control because the rail component is dominant in that frequency region. The vibration energy of the upper mass of the absorber can be seen from Fig. 5 to be higher at low frequencies up to 380 Hz, compared with the rail, but much lower at high frequencies.

The second resonance frequency of the rail absorber should be designed in the way close to the frequency at which the rail vibration and radiation reach their highest, so that the rail component of rolling noise can

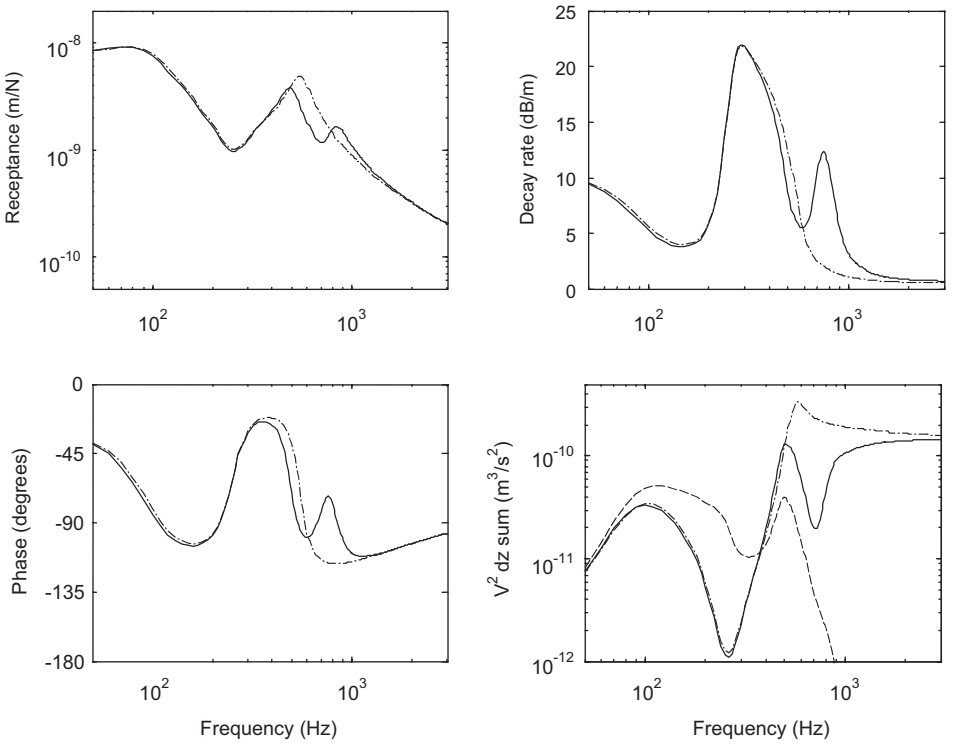

Fig. 5. Vibration receptance, decay rate and energy due to a unit excitation of the track with rail absorber for $m_1 = 14\,\text{kg/m}$, $m_2 = 6\,\text{kg/m}$, $k_1 = 260\,\text{MN/m}^2$, $k_2 = 12\,\text{MN/m}^2$, $k_3 = k_2/4$, $\eta_a = 0.25$, $f_1 = 247\,\text{Hz}$, $f_2 = 703\,\text{Hz}$: — rail with absorber, –·– rail without absorber, –– upper mass of absorber.

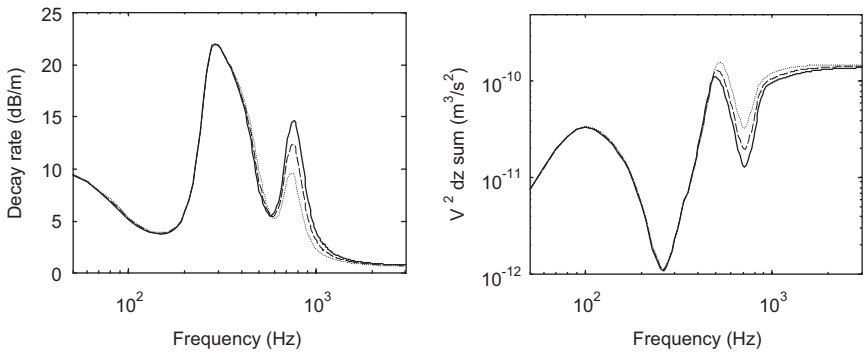

Fig. 6. Rail vibration energy and decay rate using different active mass (no change of resonance frequencies $f_1 = 247\,\text{Hz}$, $f_2 = 703\,\text{Hz}$): — $m_1 = 18.67\,\text{kg/m}$, $m_2 = 8\,\text{kg/m}$; –– $m_1 = 14\,\text{kg/m}$, $m_2 = 6\,\text{kg/m}$; ⋯ $m_1 = 9.34\,\text{kg/m}$, $m_2 = 4\,\text{kg/m}$.

effectively be reduced. To have the required resonance frequency for the absorber, theoretically, different sets of parameter can be chosen for the absorber's mass and stiffness. However, they may leads to different effects on energy reduction of rail vibration. Fig. 6 shows the influences on the decay rate and energy level of rail vibration when different active masses are used for the rail absorber, with the resonance frequencies keeping unchanged by adjusting the absorber's stiffness accordingly. The decay rate of rail vibration along the track can be found from Fig. 6 to vary with changing the mass of the absorber. The larger the mass is, the higher the decay rate around the second resonance of the absorber. Thus, the vibration energy of the rail can be seen to be lower if larger mass is used for the absorber. Although a large absorber (large mass) is beneficial to rail

noise reduction, but increase of the mass is confined by the geometrical size of the rail cross-section, where the absorber is allowed for installation. The added mass to the rail is also limited by infrastructure constraints. In this study the absorber mass including m_1 and m_2 is chosen to be 20 kg/m for the UIC 60 rail.

The rail vibration energy and decay rate are mainly affected by the second resonance of the absorber, and less affected by the first resonance. However, the vibration energy of the upper mass m_2 of the absorber is closely related to the first resonance, because m_2 is attached to the upper stiffness k_2 that is designed to be soft and determines the first resonance frequency with m_2 together. Change of k_2 independently will alter the first resonance frequency and mode shape of the absorber. The calculated results due to change of k_2 are shown in Fig. 7, with the other parameters keeping unchanged for the rail absorber: $m_1 = 14$, $m_2 = 6\,\mathrm{kg/m}$, $k_1 = 260\,\mathrm{MN/m^2}$. It can be seen form Fig. 7 that the energy and decay rate of rail vibration change only slightly, although k_2 is increased from 6 to $18\,\mathrm{MN/m^2}$, and the first resonance frequency is altered from 176 to 298 Hz. However, the vibration energy of the upper mass changes dramatically. When $k_2 = 6\,\mathrm{MN/m^2}$, the first resonance of the absorber is at 176 Hz, and the vibration energy of the upper mass is much higher than the rail around 176 Hz but much lower around 500 Hz, the second resonance frequency of the track. In contrast, when $k_2 = 18\,\mathrm{MN/m^2}$, the first resonance of the absorber is at 298 Hz, and the vibration energy of the upper mass is high in the frequency region around the first resonance of the absorber and the second resonance of the track. It can be concluded that the upper stiffness k_2 should be chosen appropriately, in order to keep the vibration energy low of the upper mass of the absorber.

The absorber damping is important for rail vibration attenuation, as the mechanism of the rail absorber is based on energy consumption at the second resonance via the elastomeric material. Different damping values are used in calculations of the track dynamics with the rail absorber. Fig. 8 depictures the influences on vibration energy and decay rate of the loss factor η_a that is chosen to be 0.15 and 0.4 for the elastomeric

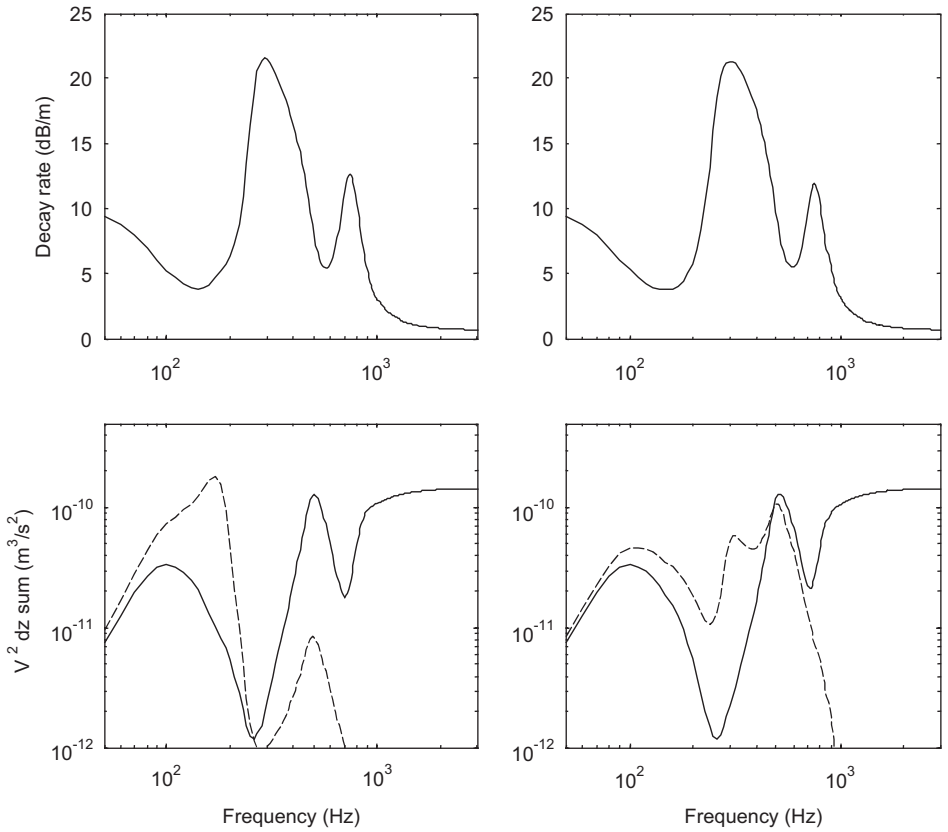

Fig. 7. Vibration energy and decay rate using different stiffness k_2, left for $k_2 = 6\,\mathrm{MN/m^2}$, $f_1 = 176\,\mathrm{Hz}$, $f_2 = 694\,\mathrm{Hz}$; right for $k_2 = 18\,\mathrm{MN/m^2}$, $f_1 = 298\,\mathrm{Hz}$, $f_2 = 713\,\mathrm{Hz}$: — rail, –– upper mass of absorber.

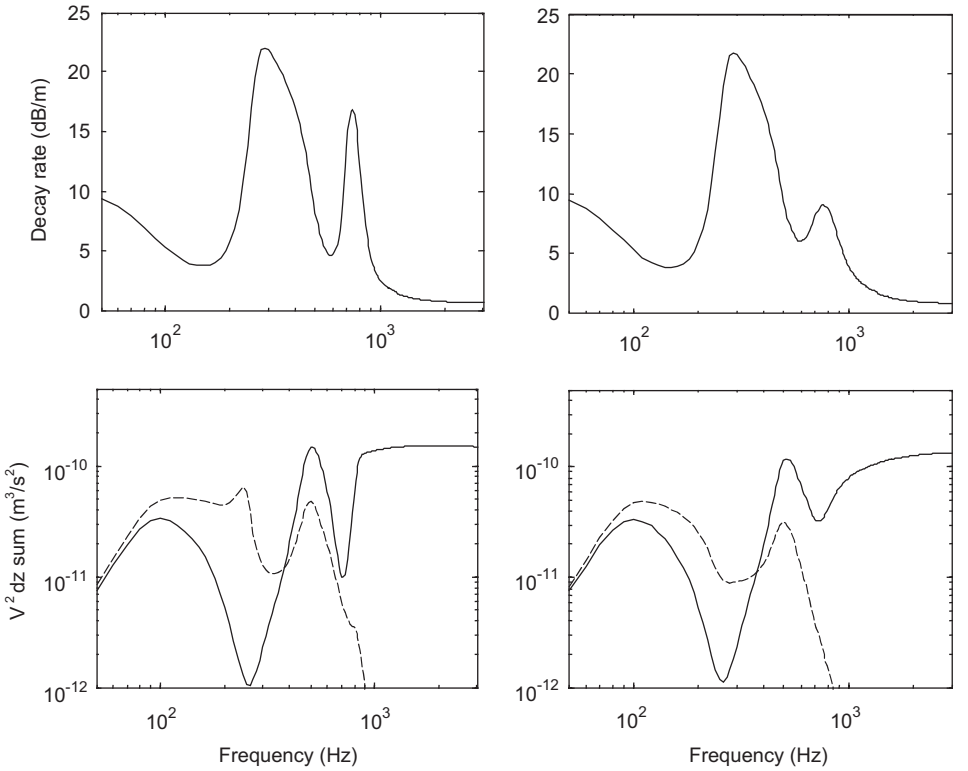

Fig. 8. Vibration energy and decay rate using different damping, left for $\eta_a = 0.15$, right for $\eta_a = 0.4$: — rail, – – upper mass of absorber.

material of the absorber. It can be seen from Fig. 8 that the decay rate goes up highly and the vibration energy comes down deeply around the second resonance of the absorber when η_a is chosen to be 0.15, but the effective frequency bandwidth of the absorber becomes narrow. When η_a is chosen to be 0.4, in contrast, the bandwidth of the decay rate peak is broadened, but the height of the peak becomes low and the effects on energy consumption are reduced. In addition, the vibration energy of the upper mass becomes high around the first resonance of the absorber when the damping is small. For the purpose of rail noise reduction, both over high and over low damping are not appropriate for the rail absorber.

3. Discrete track with continuous rail absorber

In this section, a discretely supported track model with the continuous rail absorber is developed in order to investigate the effects of the absorber on the pinned–pinned resonance of the discrete track, which cannot be characterised using the continuous track model in the previous section.

The continuous track model in Fig. 2 can also be referred to the discrete track in the way regarding the rail support as discrete rather than continuous. Treating the rail as an infinite Timoshenko beam and the attached absorber as a continuous dynamic stiffness, the equations of motion for the beam is given by

$$-\rho A\omega^2 u + GA\kappa(\phi' - u'') + k_a u + \sum_{n=1}^{N} K_s u\delta(z - z_n) = F\delta(z), \tag{11}$$

$$-\rho I\omega^2 \phi + GA\kappa(\phi - u') - EI\phi'' = 0, \tag{12}$$

where k_a is the dynamic stiffness of the rail absorber and given by Eq. (10), N is the number of the rail support considered in the model, z_n represents the sleeper position and K_s is the dynamic stiffness of the discrete

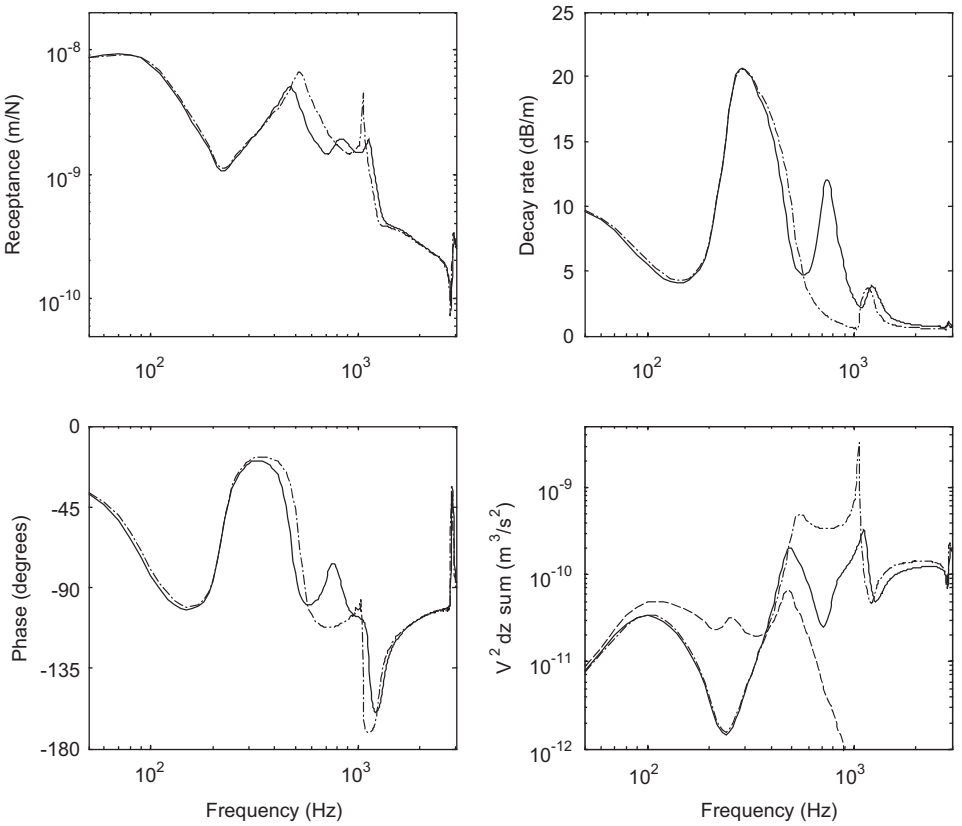

Fig. 9. Vibration receptance, decay rate and energy of discrete track with continuous rail absorber due to a unit harmonic excitation at mid-span for $m_1 = 14\,\mathrm{kg/m}$, $m_2 = 6\,\mathrm{kg/m}$, $k_1 = 260\,\mathrm{MN/m^2}$, $k_2 = 12\,\mathrm{MN/m^2}$, $k_3 = k_2/4$, $\eta_a = 0.25$, $f_1 = 247\,\mathrm{Hz}$, $f_2 = 703\,\mathrm{Hz}$: — rail with absorber, $-\cdot-$ rail without absorber, $--$ upper mass of absorber.

support of the track, given by

$$K_s = \frac{K_p(K_b - M_s\omega^2)}{K_p + K_b - M_s\omega^2}, \tag{13}$$

where M_s is the sleeper mass, K_p and K_b are the pad and ballast stiffness respectively. The discrete parameters M_s, K_p and K_b can be obtained by multiplying the continuous parameters m_s, k_p and k_b by the sleeper span length d that is chosen to be 0.6 m for the discrete track support.

To solve Eqs. (11) and (12) the concept of vibration receptance of the rail with the absorber is used. The cross receptance $\alpha(z_2, z_1)$ for the rail with the attached absorber is defined as the displacement response at $z = z_2$ caused by a unit harmonic force at $z = z_1$. Then the rail displacement $u(z)$ can be calculated by

$$u(z) = F\alpha(z, 0) - \sum_{n=1}^{N} K_s u(z_n)\alpha(z, z_n). \tag{14}$$

It can be realized from Eq. (14) that the track displacement is the result of superposition caused by the oscillating load F and the resilient force of the rail support $K_s u(z_n)$. The details of calculation of the vibration receptance of the rail with the attached absorber are referred in the appendix.

According to Eq. (14), the rail vibration displacement at the support position $z = z_j$ can be calculated by

$$u(z_j) = F\alpha(z_j, 0) - \sum_{n=1}^{N} K_s u(z_n)\alpha(z_j, z_n), \quad j = 1, 2, \ldots, N. \tag{15}$$

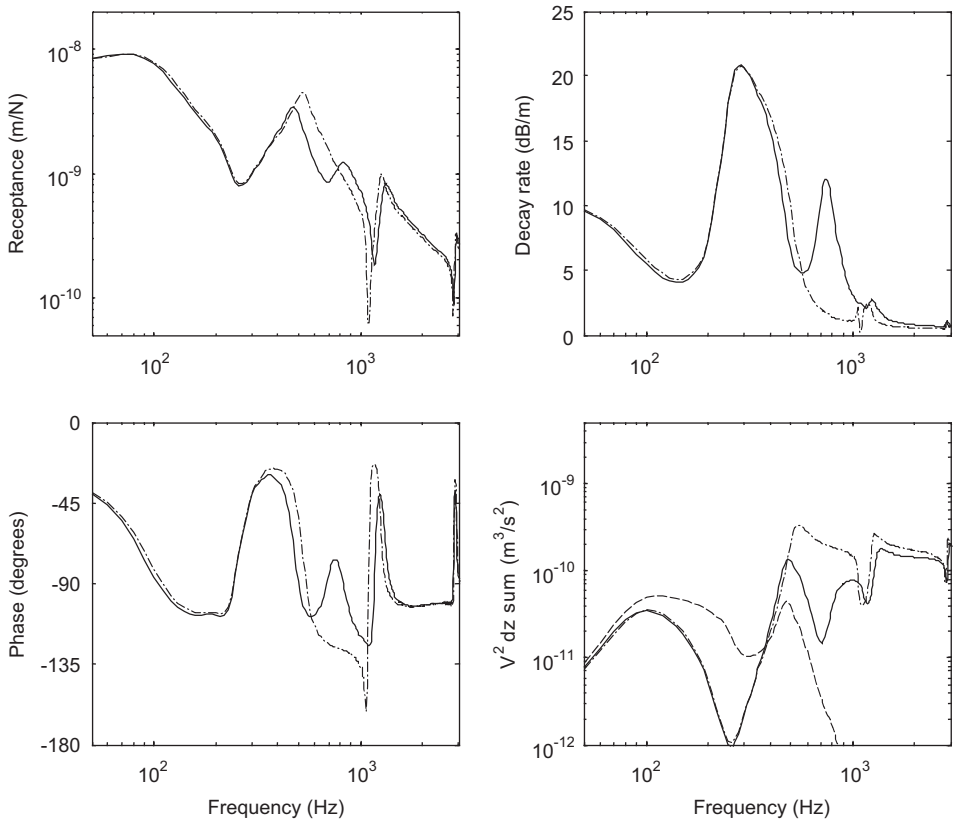

Fig. 10. Vibration receptance, decay rate and energy of discrete track with continuous rail absorber due to a unit harmonic excitation above a sleeper, keys as for Fig. 9.

After the displacement at the support being worked out using Eq. (15), the rail vibration displacement at any point can be calculated by substituting $u(z_j)$ for $u(z_n)$ in Eq. (14). The vibration displacement of the absorber mass can be calculated using Eqs. (6) and (7). The concept of the discrete track model and the formulation were originally established by Heckl [13], and similar methodology was used in Ref. [14] for high-frequency vibration of the refined track model. Further, for the theory and method of analyzing periodic structures, Mead's work [15] can be referred to.

The calculated dynamic properties of the discretely supported track with the continuous absorber are shown in Figs. 9 and 10 for a unite harmonic load at mid-span and above a sleeper, respectively, in terms of the point receptance, decay rate of rail vibration along the track and the energy of vibration of the rail and upper mass of the absorber. The same parameters of the rail absorber as used for the continuous track are applied to the discrete track. The pinned–pinned resonance can be observed from Figs. 9 and 10 to be at about 1050 Hz, which corresponds to a standing wave with nodes at the sleepers and peaks at mid-spans. The point receptance at mid-span reaches a very sharp peak at the pinned–pinned resonance frequency for the track without the absorber, and thus the energy of rail vibration also reaches a sharp peak. This phenomenon cannot be observed when the continuous track model is used. It can be seen from Figs. 9 and 10 that the peaks in the receptance and vibration energy of the rail due to the pinned–pinned resonance can effectively be suppressed by use of the rail absorber, and thus the rail vibration and radiation can be reduced.

4. Discrete track with discrete rail absorber

The rail absorber can be devised to be either continuous or discrete attached to the rail. The discrete rail absorber may be installed at different positions along the track, for example at mid-span of a sleeper bay and

at a sleeper. Which one is more effective of the continuous and discrete absorber and, where is the most appropriate place for installation of the discrete absorber for the target of rail vibration and noise reduction? The questions remain to be answered.

In this section, the effectiveness of the discrete rail absorber is investigated and compared to that of the continuous absorber. Also investigated is the influence of the installation position of the absorber. Two places are taken into consideration, at mid-span of a sleeper bay and above a sleeper.

The model of the discrete track with the discrete absorber is different from the models developed for the continuous absorber attached to the continuous or discrete track. It is developed in the base of an infinite Timoshenko beam for the rail, with the track support and the rail absorber being regarded as the discrete forces to the rail. The equation of motion for the infinite rail is given by

$$-\rho A\omega^2 u + GA\kappa(\phi' - u'') + \sum_{m=1}^{M} K_a u\delta(z - z_m) + \sum_{n=1}^{N} K_s u\delta(z - z_n) = F\delta(z), \tag{16}$$

$$-\rho I\omega^2\phi + GA\kappa(\phi - u') - EI\phi'' = 0, \tag{17}$$

where M and N are the number of the discrete absorber and support considered, respectively, z_m represents the installation position of the absorber that is either at mid-span or above a sleeper, z_n represents the sleeper position ($z_m = z_n$ when the absorber is installed at a sleeper), K_s is the dynamic stiffness of the discrete support,

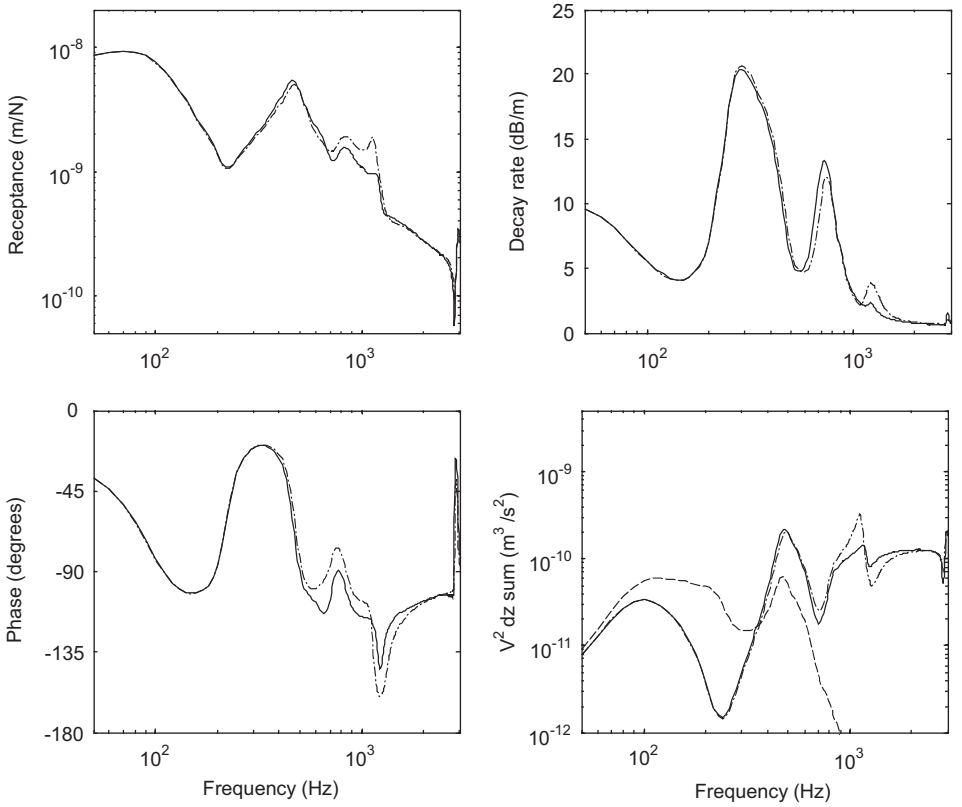

Fig. 11. Vibration receptance, decay rate and energy of discrete track with discrete rail absorber at mid-span due to a unit harmonic excitation at mid-span for $M_1 = 8.4\,\text{kg}$, $M_2 = 3.6\,\text{kg}$, $K_1 = 156\,\text{MN/m}$, $K_2 = 7.2\,\text{MN/m}$, $K_3 = K_2/4$, $\eta_a = 0.25$, $f_1 = 247\,\text{Hz}$, $f_2 = 703\,\text{Hz}$: — rail with discrete absorber, –·– rail with continuous absorber, –– upper mass of absorber.

refer to Eq. (13), and K_a is the dynamic stiffness of the discrete absorber, given by (refer to Eq. (10))

$$K_a = K_1\left\{1 - \frac{K_1(K_2+K_3-M_2\omega^2)+K_2K_3}{(K_1+K_2-M_1\omega^2)(K_2+K_3-M_2\omega^2)-K_2^2}\right\} + K_3\left\{1 - \frac{K_3(K_1+K_2-M_1\omega^2)+K_1K_2}{(K_1+K_2-M_1\omega^2)(K_2+K_3-M_2\omega^2)-K_2^2}\right\}. \quad (18)$$

The parameters of the discrete absorber M_1, M_2, K_1, K_2, and K_3 can be obtained by multiplying the continuous parameters m_1, m_2, k_1, k_2, and k_3 by the sleeper span length d.

Using the concept of cross receptance of the rail, $\beta(z_2, z_1)$, the rail vibration displacement $u(z)$ can be calculated by

$$u(z) = F\beta(z,0) - \sum_{m=1}^{M} K_a u(z_m)\beta(z,z_m) - \sum_{n=1}^{N} K_s u(z_n)\beta(z,z_n). \quad (19)$$

Substituting z_j for z in Eq. (19), the rail displacement at the position of the absorber and support is given by

$$u(z_j) = F\beta(z_j,0) - \sum_{m=1}^{M} K_a u(z_m)\beta(z_j,z_m) - \sum_{n=1}^{N} K_s u(z_n)\beta(z_j,z_n), \quad j = 1,2,\ldots,N+M. \quad (20)$$

Then substituting the rail displacement $u(z_j)$ calculated from Eq. (20) for $u(z_m)$ and $u(z_n)$ in Eq. (19), the displacement of the rail at any point can be obtained. The displacements of the absorber masses can be calculated using Eqs. (6) and (7), but the parameters of the discrete absorber, M_1, M_2, K_1, K_2, and K_3, should be used.

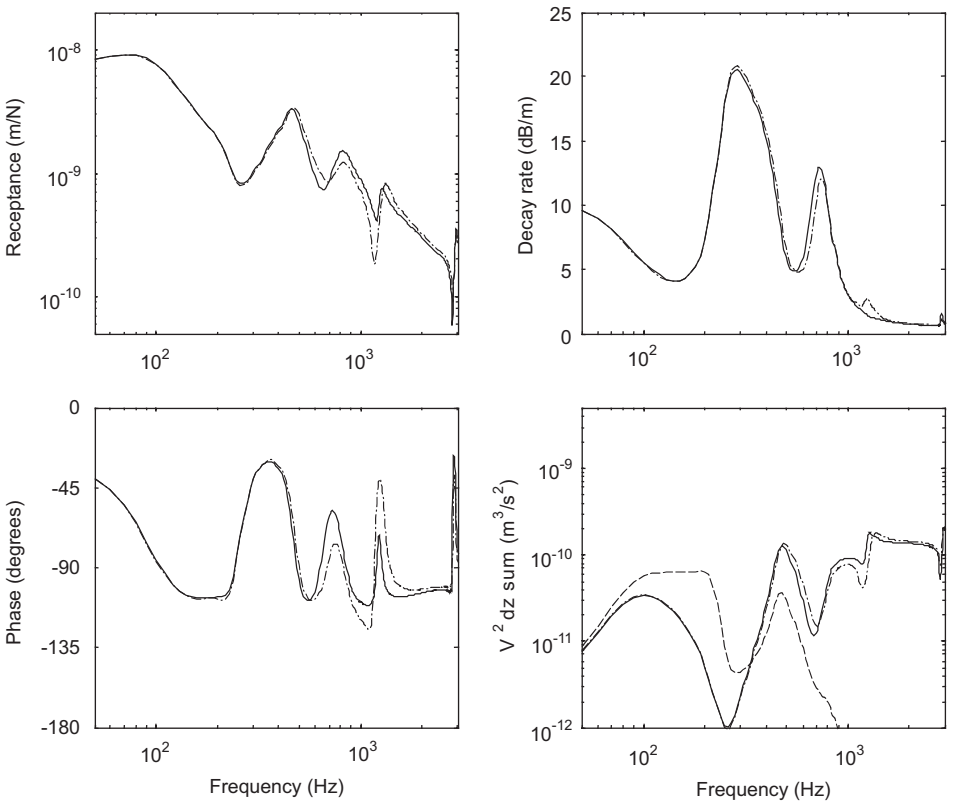

Fig. 12. Vibration receptance, decay rate and energy of discrete track with discrete rail absorber at mid-span due to a unit harmonic excitation above a sleeper, keys as for Fig. 11.

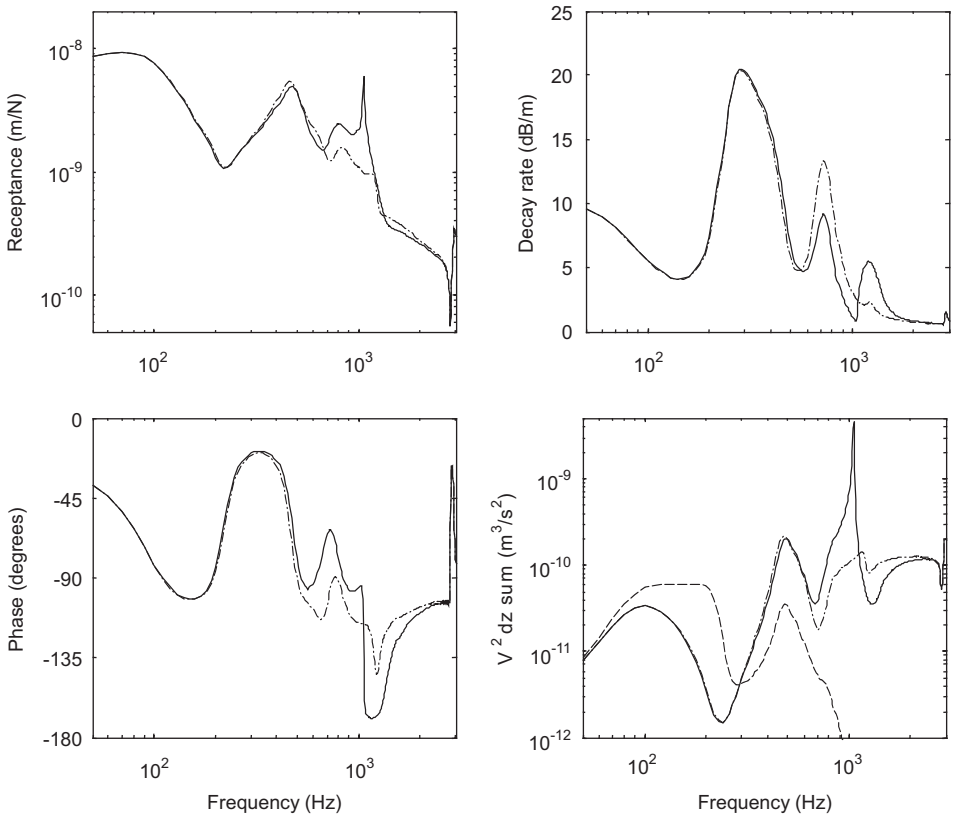

Fig. 13. Vibration receptance, decay rate and energy of discrete track with discrete rail absorber at sleeper due to a unit harmonic excitation at mid-span for $M_1 = 8.4\,\text{kg}$, $M_2 = 3.6\,\text{kg}$, $K_1 = 156\,\text{MN/m}$, $K_2 = 7.2\,\text{MN/m}$, $K_3 = K_2/4$, $\eta_a = 0.25$: — rail with absorber at sleeper, –·– rail with absorber at mid-span, –– upper mass of absorber.

The parameters for the discrete absorber used in the calculations are corresponding to the continuous ones, to make the results comparable between the continuous and discrete absorber. The calculation results for the discrete rail absorber at mid-span of a sleeper bay are shown in Figs. 11 and 12 for the unite harmonic load at mid-span and above a sleeper, respectively. Compared with the track with the continuous absorber, the dynamic properties are similar, but the vibration energy of the rail can be reduced further at the pinned–pinned resonance when the discrete rail absorber is installed at mid-span and the excitation is also applied there.

Figs. 13 and 14 show the calculation results from the track using the discrete rail absorber at a sleeper with the excitation at mid-span and above a sleeper, respectively. The decay rate of rail vibration can be seen from Figs. 13 and 14 to be lower at the second resonance of the absorber than that of the track with the absorber at mid-span of a sleeper bay, even lower than the track with the continuous absorber. Although the decay rate just above the pinned–pinned resonance is a bit higher, the peak in the vibration energy at the pinned–pinned resonance cannot be suppressed by the discrete absorber at a sleeper when the excitation is at mid-span. This is because at the pinned–pinned resonance the nodes of rail vibration are at the sleepers, where the vibration amplitude is low and thus the rail absorber there cannot function well as the energy consumer. It can be conclude that it is not a right place at a sleeper for installation of the discrete rail absorber.

5. Conclusions

The mechanism of vibration reduction via energy consumption by the rail absorber is studied. A continuous model of the track combined with the rail absorber is developed for analysis of vertical dynamics of the track. Using the combined track model the influences on vibration decay along the track are investigated of the

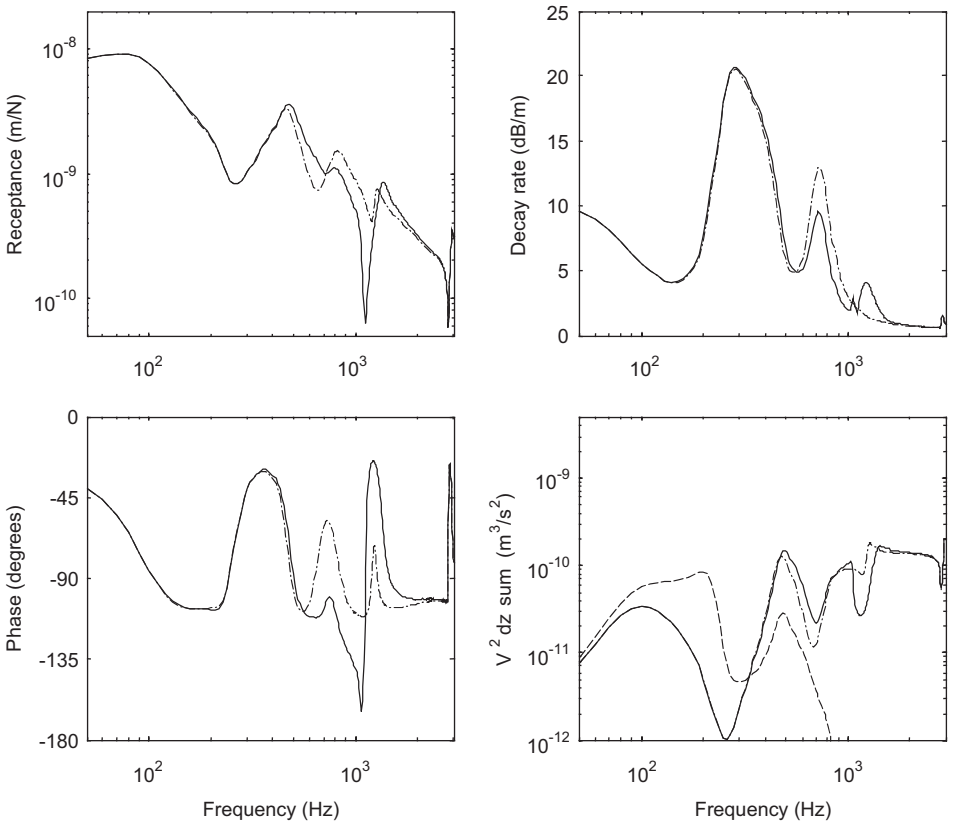

Fig. 14. Vibration receptance, decay rate and energy of discrete track with discrete rail absorber at sleeper due to a unit harmonic excitation above a sleeper, keys as for Fig. 13.

parameters of the rail absorber. In addition, the discrete track models combined with both the continuous and discrete rail absorber are developed to calculate their effectiveness on vibration decay. Moreover, the influences on vibration decay are studied of the two different installation positions for the discrete absorber, which are in the middle of sleeper span and at a sleeper.

The calculation results show that a large active mass used in the absorber is beneficial to attenuation of rail vibration. Over high or over low loss factor of the damping material used in the absorber may degrade its performance on rail vibration reduction. The most effective installation position for the discrete absorber is in the middle of sleeper span because where the vibration amplitude is high and the pinned–pinned resonance can be damped. The effectiveness of the piecewise continuous absorber installed along the rail is moderate compared with the discrete absorber installed in the middle of sleeper span and at a sleeper. The place at a sleeper is not appropriate to arrange the discrete absorber, as the vibration amplitude there is flat.

Further, the compound track model developed can be combined with the sound radiation model, the wheel/rail interface and the roughness input, which are available within the TWINS model [16], for predicting the effects of the rail absorber on rolling noise reduction.

Appendix

The equations of motion for the rail (infinite Timoshenko beam) with the continuous absorber attached are given by

$$-\rho A\omega^2 u + GA\kappa(\phi' - u'') + k_a u = 0, \tag{A.1}$$

$$-\rho I\omega^2 \phi + GA\kappa(\phi - u') - EI\phi'' = 0, \tag{A.2}$$

where u is the vertical displacement of the beam and ϕ is the rotation of cross-section of the beam due to bending. $\phi - u'$ represents the shear deformation and $'$ indicates the derivative with respect to z, the longitudinal coordinates of the beam. The material properties are described by E, the Young's modulus, G, the shear modulus, and ρ, the density. The geometric properties of the cross-section are characterised by A, the cross-sectional area, I, the area moment of inertia, and κ, the shear coefficient. k_a is the dynamic stiffness of the rail absorber, given as

$$k_a = k_1\left\{1 - \frac{k_1(k_2+k_3-m_2\omega^2)+k_2k_3}{(k_1+k_2-m_1\omega^2)(k_2+k_3-m_2\omega^2)-k_2^2}\right\} + k_3\left\{1 - \frac{k_3(k_1+k_2-m_1\omega^2)+k_1k_2}{(k_1+k_2-m_1\omega^2)(k_2+k_3-m_2\omega^2)-k_2^2}\right\}, \tag{A.3}$$

where m_1, m_2, k_1, k_2, and k_3 are the parameters of the absorber. Damping can be added by making the stiffness complex in the form $k(1+i\eta)$.

For the infinite Timoshenko beam with a unite oscillating force applied at the middle of the beam, $z = 0$, the boundary conditions at $z = 0$ are given as

$$\phi(0) = 0, \tag{A.4}$$

$$u'(0) - \phi(0) = -\frac{1}{2GA\kappa}, \tag{A.5}$$

where the bending rotation $\phi(0) = 0$ rather than the slope of the central line of the beam $u'(0) = 0$, this is because the shear deformation of the Timoshenko beam $\phi - u'$ is discontinuous at the forcing point $z = 0$, although the beam deformation is symmetric about the forcing point.

Assuming $u = Ue^{sz}$ and $\phi = \Phi e^{sz}$, substituting them into Eqs. (A.1) and (A.2) and combining them in the form of matrix equation result in

$$\begin{bmatrix} k_a - \rho A\omega^2 - GA\kappa s^2 & GA\kappa s \\ -GA\kappa s & GA\kappa - \rho I\omega^2 - EIs^2 \end{bmatrix} \begin{Bmatrix} U \\ \Phi \end{Bmatrix} = \mathbf{0}. \tag{A.6}$$

The equation for s in terms of ω can be obtained by equating the determinant of the matrix to zero, the condition under which there is a nontrivial solution to Eq. (A.6). Since damping is introduced by loss factors, s appears in two pairs of complex. One pair is for wave propagation in the positive direction, and the other in the negative direction. Supposing $s = k_1$ and $s = k_2$, whose real part is negative, are for wave propagation in the positive direction, then the vertical displacement u and rotation ϕ can be given as

$$u = B_1e^{k_1z} + B_2e^{k_2z}, \tag{A.7}$$

$$\phi = C_1e^{k_1z} + C_2e^{k_2z}. \tag{A.8}$$

As C_1 can be solved in terms of B_1, and C_2 in terms of B_2 by making use of either pairs of equation from Eq. (A.6), this yields

$$C_1 = B_1\frac{k_1GA\kappa}{GA\kappa - \rho I\omega^2 - k_1^2EI}, \tag{A.9}$$

$$C_2 = B_2\frac{k_2GA\kappa}{GA\kappa - \rho I\omega^2 - k_2^2EI}. \tag{A.10}$$

The boundary conditions given by Eqs. (A.4) and (A.5) should be satisfied when the unite oscillating load is applied to the beam at $z = 0$, and this leads to the following solution for B_1 and B_2:

$$B_1 = \frac{1}{2GA\kappa(k_2b_1/b_2 - k_1)}, \tag{A.11}$$

$$B_2 = \frac{1}{2GA\kappa(k_1 b_2/b_1 - k_2)}, \tag{A.12}$$

where

$$b_1 = \frac{k_1 GA\kappa}{GA\kappa - \rho I\omega^2 - k_1^2 EI}, \tag{A.13}$$

$$b_2 = \frac{k_2 GA\kappa}{GA\kappa - \rho I\omega^2 - k_2^2 EI}. \tag{A.14}$$

As the longitudinal dimension z is infinite, the cross receptance, $\alpha(z_1, z_2)$, of the rail with the attached absorber can be obtained by substituting $|z_1–z_2|$ for z in Eq. (A.7), and given by

$$\alpha(z_1, z_2) = B_1 e^{k_1|z_1-z_2|} + B_2 e^{k_2|z_1-z_2|}. \tag{A.15}$$

The cross receptance of an infinite Timoshenko beam, $\beta(z_1, z_2)$, can be obtained through the same procedure by taking $k_a = 0$ in Eqs. (A.1) and (A.6).

References

[1] P.J. Remington, Wheel/rail rolling noise I: theoretical analysis, *Journal of the Acoustical Society of America* 81 (1987) 1805–1823.

[2] P.J. Remington, Wheel/rail rolling noise, II: validation of the theory, *Journal of the Acoustical Society of America* 81 (1987) 1824–1832.

[3] D.J. Thompson, Wheel–rail noise generation, part I: introduction and interaction model, *Journal of Sound and Vibration* 161 (1993) 387–400.

[4] D.J. Thompson, B. Hemsworth, N. Vincent, Experimental validation of the TWINS prediction program for rolling noise, part 1: description of the model and method, *Journal of Sound and Vibration* 193 (1996) 123–135.

[5] D.J. Thompson, P. Fodiman, H. Mahé, Experimental validation of the TWINS prediction program for rolling noise, part 2: results, *Journal of Sound and Vibration* 193 (1996) 137–147.

[6] C.J.C. Jones, D.J. Thompson, R.J. Diehl, The use of decay rates to analyse the performance of railway track in rolling noise generation, *Journal of Sound and Vibration* 293 (2006) 485–495.

[7] D.J. Thompson, P.-E. Gautier, Review of research into wheel/rail rolling noise reduction, *Proceedings of the Institution of Mechanical Engineers Part F: Journal of Rail and Rapid Transitions* 220 (2006) 385–408.

[8] D.J. Thompson, C.J.C. Jones, T.X. Wu, G. de France, The influence of the non-linear stiffness behaviour of rail pads on the track component of rolling noise, *Proceedings of the Institution of Mechanical Engineers Part F: Journal of Rail and Rapid Transitions* 213 (1999) 233–241.

[9] N. Vincent, P. Bouvet, D.J. Thompson, P.E. Gautier, Theoretical optimization of track components to reduce rolling noise, *Journal of Sound and Vibration* 193 (1996) 161–171.

[10] D.J. Thompson, C.J.C. Jones, T.P. Waters, D. Farrington, A tuned damping device for reducing noise from railway track, *Applied Acoustics* 68 (2007) 43–57.

[11] F. Ltourneaux, F. Margiocchi, F. Poisson, Complete assessment of rail absorber performances on an operated track in France, *Proceedings of World Congress on Railway Research*, Montreal, Canada, 2006, CDROM.

[12] J. Maes, H. Sol, A double tuned rail damper-increased damping at the two first pinned–pinned frequencies, *Journal of Sound and Vibration* 267 (2003) 721–737.

[13] M.A. Heckl, Railway noise—can random sleeper spacing help?, *Acustica* 81 (1995) 559–564.

[14] T.X. Wu, D.J. Thompson, Vibration analysis of railway track with multiple wheels on the rail, *Journal of Sound and Vibration* 239 (2001) 69–97.

[15] D.J. Mead, A new method of analyzing wave propagation in periodic structures; applications to periodic Timoshenko beams and stiffened plates, *Journal of Sound and Vibration* 104 (1986) 9–27.

[16] D.J. Thompson, M.H.A. Janssens, *TWINS: Track–Wheel Interaction Noise Software, Theoretical Manual (Version 2.4)*, TNO Institute of Applied Physics Report TPD-HAG-RPT-93-0214, Delft, 1997.